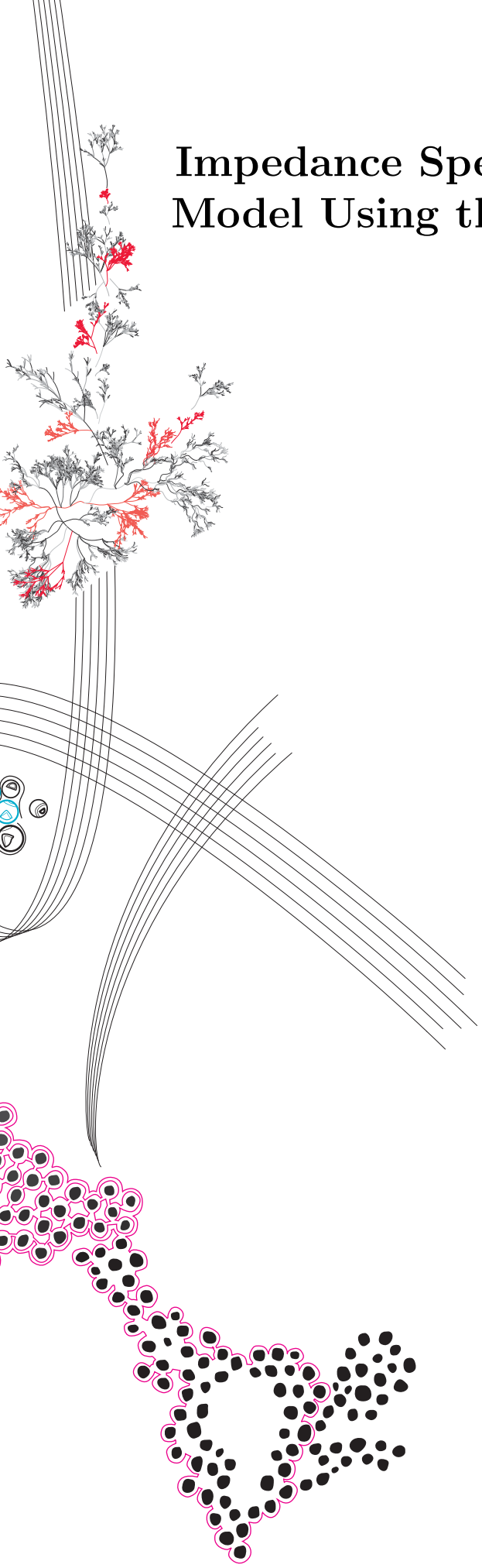

Impedance Spectroscopy of Retina-on-Chip Model Using the Custom-Designed Artemis System

30-06-2025

Sarah Tromp
Prof.dr Andries van der Meer
ir. Devin Veerman
Prof.dr.ir. Loes Segerink

University of Twente
Science & Technology

Summary

In this study, impedance spectroscopy was applied to a Retina-on-Chip (RoC) model using the custom-designed Locsense Artemis ST system. The aim was to evaluate the system's usability for monitoring the integrity of an ARPE-19 cell monolayer in preparation for future experiments. Barrier integrity is a critical parameter for studying drug delivery across the outer blood–retina barrier (oBRB), particularly in the context of retinal diseases such as age-related macular degeneration (AMD). Organ-on-a-Chip (OoC) models offer a promising alternative to animal models by mimicking key aspects of human physiology, yet they require non-invasive and reliable methods to assess barrier function.

Recent technological advances have enabled the integration of electrodes into microfluidic chips, facilitating transepithelial electrical resistance (TEER) measurements via impedance spectroscopy. This label-free technique allows continuous, in vitro monitoring of barrier properties. However, measurement equipment must often be tailored to the specific layout and requirements of the chip. Although the Artemis system was developed for such applications, its compatibility and performance required validation.

Validation experiments confirmed expected impedance trends with varying ion concentrations and membrane presence. However, in cell culture experiments, impedance values were higher than expected, indicating the need for further investigation into the system's sensitivity and calibration.

Contents

1 Introduction

Retinal diseases may lead to severe vision loss or blindness. The most leading cause for blindness is age-related macular degeneration (AMD). Currently it effects over 200 million people worldwide with the expection to be 288 million in 2040 [1, 2].

In AMD, loss of retinal pigment epithelium (RPE) precedes degeneration of neural retina. The RPE plays many supportive roles for photoreceptors, such as the formation of the blood-retina barrier (BRB), nutrients and oxygen supply, recycling of photoreceptors and clearing waste products [3].

The human eye has multiple layers with different cells to convert light into an electrical signal. It is organized into three main nuclear layers containing different type of cells, see Figure 1. The outer nuclear layer contains the photoreceptors, rods and cones, whose outer segments initiate phototransduction through opsin-rich disk membranes. Signals from the photoreceptors are transmitted to the inner nuclear layer, which contains bipolar, horizontal, and amacrine cells that modulate and process visual input. These signals are then passed to the retinal ganglion cell (RGC) layer, where ganglion cells integrate and transmit the signals through their axons [1].

Müller glial cells provide structural and metabolic support for the whole retina. Underlying the neural retina is the RPE, forming together with Bruch's membrane and the choroid the outer blood–retina barrier (oBRB). Within the retina itself, the inner blood–retina barrier (iBRB) is formed by endothelial cells [1].

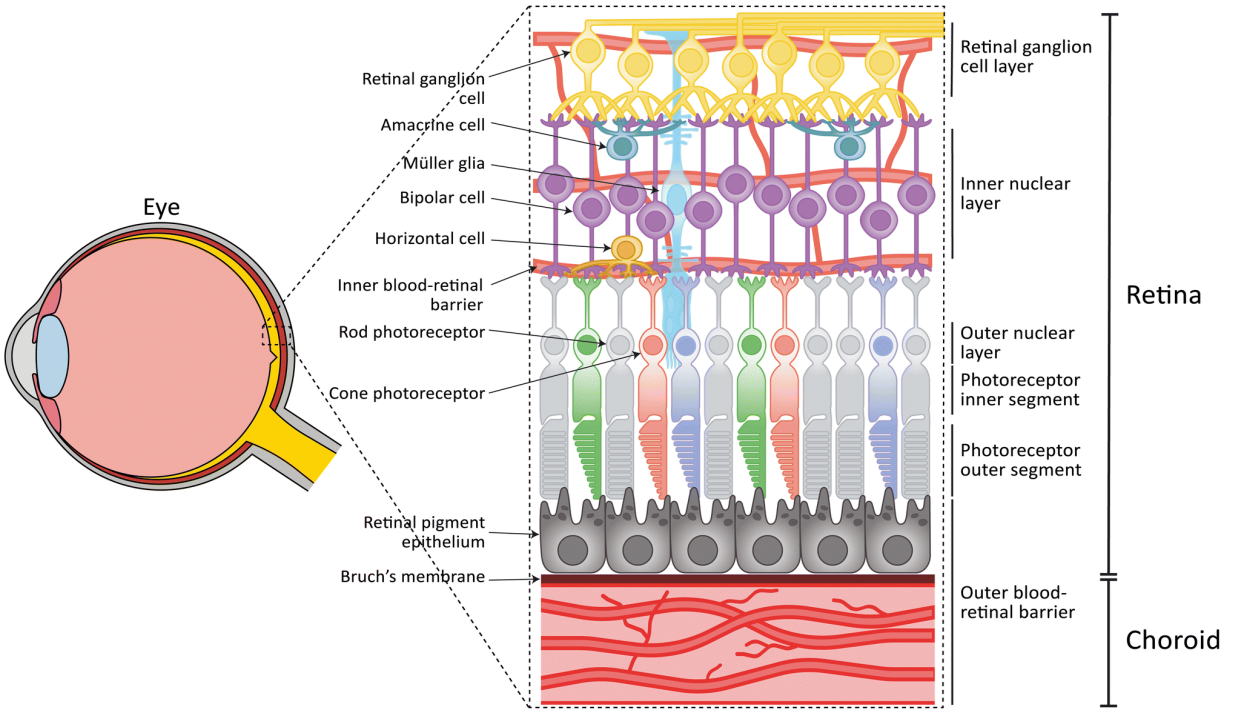

Figure 1: The anatomy of the eye with the three main nuclear layers of the retina. The outer nuclear layer contains the rod and cone photoreceptor cells. Bipolar cells, horizontal cells, amacrine cells and Müller glia lay in the inner nuclear layer, and retinal ganglion cells in the retinal ganglion cell layer. The RPE, Bruch's membrane, and the choroid form the oBRB. A vasculature surrounding the inner retinal layers form the iBRB [1].

In order to produce effective medication to treat AMD, it is necessary to understand drug transport into the retina. For systemic administration drugs in particular the BRB is important, since this regulates fluids and molecular movement between the ocular vascular beds and retinal tissue [4]. In the outer layer the RPE cells are connected with tight junctions. The tight junctions mainly regulate paracellular diffusion and are essential for barrier integrity and cell polarity [4].

1.1 Organ-on-a-Chip

The golden standard for preclinical drug testing is now conducted on animal models, such as rodents. However, differences in morphology and lack of specific phenotypes for the human disease can result in misleading outcomes [1]. Approximately 40% of the drugs tested on animal models will fail clinical trials [5]. For this reason, advances are made to microfluidic Organ-on-a-Chip technique for improvement in drug testing and replacing animal testing. An Organ-on-a-Chip (OoC) is a microphysiological system that mimics the physiology and functionality of human organs, without reproducing the whole tissue [5]. It focuses on mimicking the key components that reflect the function and physiology of the organ needed for drug testing. Advantages of OoC include the possibility to maintain chemical and mechanical tissue properties and the guarantee of reproducibility. This makes it a cost effective and reliable method to control parameters [6, 7].

1.2 Measuring with sensors

Electrodes and sensors can be integrated in a chip, making it possible to detect biological signals while real-time monitoring living cells [8]. One important application with electrodes on a chip is the transepithelial electrical resistance (TEER). This is a non-invasive quantitative method that is used to evaluate ion transport and tightness of the tight junctions of epithelial/endothelial tissue or monolayer cells.

There are two methods to determine the TEER value, Ohm's law and the impedance spectroscopy [7, 9]. This research focuses on the method using impedance spectroscopy. When a correct algorithm is used, this method results in a more accurate TEER value than the method which determines the value using Ohm's law [7, 9].

The electrical impedance is determined by measuring the amplitude and phase shift of the resulting current of the small amplitude AC excitation signal with a frequency sweep. From the impedance spectrum it is possible to determine the TEER value and capacity of the cellular monolayer, following the method described below [7, 9].

A way to determine the TEER value and capacity of the cellular monolayer is with an equivalent electrical circuit analysis [7]. Figure 2a shows an equivalent circuit. The current flows through the medium, where it encounters the resistance of the medium (R_{medium}), and can either flow through the junction between the cells (paracellular route) or through the cell membrane of the cells (transcellular route). In the paracellular route, the tight junctions contribute to an ohmic resistance (R_{TEER}). In the transcellular route, each lipid bilayer contributes to a parallel circuit consisting of an ohmic resistance ($R_{membrane}$) and an electrical capacitance (C_C). Finally, the current encounters the capacitance of the electrodes ($C_{electrodes}$). Since the high values of $R_{membrane}$ cause the current to mostly flow across C_C, it is possible to simplify the circuit as shown in Figure 2b [7].

With the simplified electrical circuit and the real and imaginary part of the impedance, Equation 1.1, it is possible to find the circuit parameters by fitting the experimental data to the circuit using non-linear least squares fitting techniques [7].

$$|Z| = Z_R + jZ_I \tag{1.1}$$

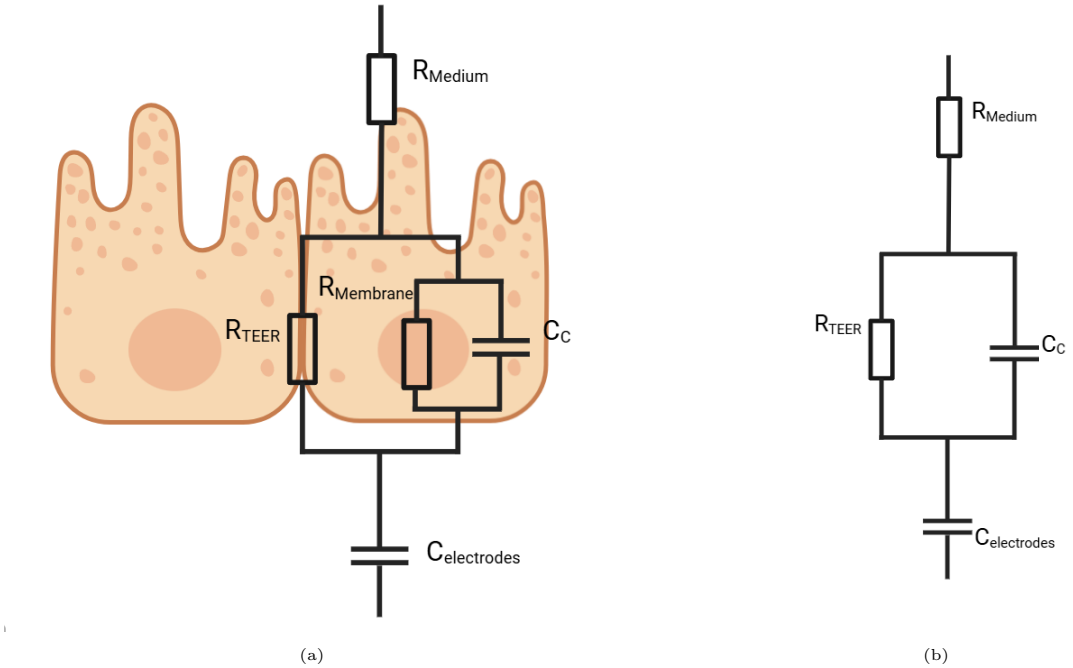

(a) (b)

Figure 2: (a) Equivalent electrical circuit for the cellular monolayer when conducting impedance measurements with the resistance of the medium (R_{medium}), ohmic resistance of the tight junctions (R_{TEER}), ohmic resistance ($R_{membrane}$) and an electrical capacitance (C_C) from each lipid bilayer and the capacitance of the electrodes ($C_{electrodes}$). (b) A simplified version of the electrical circuit, where high values of $R_{membrane}$ cause the current to flow across C_C.

An impedance spectrum can be split into three frequency regions where the impedance is dominated by certain equivalent circuit elements, see Figure 3 [7]. The low frequency range is dominated by $C_{electrodes}$, mid frequency range by R_{TEER} and C_C and high frequency range is dominated by R_{medium}. This means that the mid frequency range is dominated by elements regarding the cells.

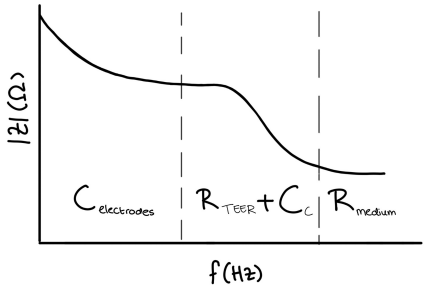

Figure 3: Impedance spectrum showing three frequency ranges, each dominated by different circuit elements. At low frequencies, $C_{electrodes}$ dominates. The mid-frequency range is governed by R_{TEER} and C_C. At high frequencies, R_{medium} is the dominant element.

With a Transwell plate two electrodes are placed on both sides of the cellular monolayer cultured on a semipermeable membrane. These type of electrodes are called “chopstick” electrodes. When using the chopstick electrodes, placement is important [7, 9]. Stability and correct placement of the electrodes is needed to measure the same impedance spectrum. If not done consistently, this method results in unprecise measurements. Besides, chopstick electrodes are impractical for OoCs since the cell culture area in the chip is too small to properly place the electrodes and the chip is not always open to place the electrodes [10]. That is why there are different special designed chips with integrated electrodes for impedance measurements.

1.3 Importants of TEER with barrier cells

To develop a model of the outer blood-retina barrier (oBRB) in retina-on-chip systems, RPE cells have been employed in various studies. The most relevant cell line is the induced pluripotent stem cell-derived RPE (iRPE), as these cells are capable of maturing, exhibit strong barrier resistance, and display pigmentation characteristics similar to native RPE cells [1].

However, to ensure the reliability of in vitro experiments, it is crucial to evaluate the model's physiological accuracy. Specifically for the oBRB, it is essential that the cultured barrier demonstrates integrity and permeability properties that closely mimic those of the native human barrier [7].

An immunostaining can be conducted for the proteins of the tight junction regarding their presence to validate the barrier integrity [10]. For testing the permeability, paracellular tracer compounds of different molecular weights with radioactive or fluorescent tracers can be used [9]. A disadvantage of the tracer compounds is that they can interfere with the integrity. The barrier is not representative anymore for the human eye barrier, making it not suitable for the drug transport experiment. A disadvantage of immunostaining is that with this method the cells are fixated and fluorescense is bound with antibodies. Since the cells are fixated, something is shown at a one time moment and the sample is unusable for further experiments [7, 10].

TEER enables the possibility to determine the barrier integrity and permeability by measuring electrical resistance across cellular monolayer. This method can be used to monitor live cells and their differentiation without damaging them, keeping them usable for further experiments [7, 9].

1.4 State of art

Traditionally, impedance measurements are performed using Transwell inserts combined with two "chopstick" electrodes placed on either side of a porous membrane. While this method is well-established, it has several limitations, including low spatial resolution, manual variability, and limited physiological relevance [11, 12, 13].

In recent years, an increasing number of microfluidic chips with integrated electrodes have been developed, as Organ-on-Chip (OoC) technology has emerged as a promising alternative. These platforms aim to recreate more realistic microenvironments and tissue functions, offering a more physiologically relevant approach [6, 7].

Despite this technological progress, a clear standard for reliable, chip-based TEER measurements

is still lacking, both in terms of methodology and specialized equipment. Many existing OoC with integrated electrodes either do not support TEER measurements at all or face technical challenges due to microscale geometry, integration complexity, or suboptimal electrode positioning [14]. Moreover, the diversity in chip and electrode designs makes it difficult to compare TEER values across systems [15].

As a result, further research is needed to evaluate emerging systems, identify technical limitations, and establish practical protocols for accurate and reproducible impedance measurements on-chip.

1.5 Aim of this study

Since measuring impedance on a chip is a relatively new and technically challenging method, it requires specially designed chips and equipment. In this research, impedance measurements were performed using a chip–system combination specifically developed for retinal barrier models. The main objective was to assess the usability of the Locsense Artemis ST system for impedance measurements and ion concentration testing, in preparation for future experiments. Due to the unavailability of iRPE cells, ARPE-19 cells were used to evaluate the impedance spectrum. Although ARPE-19 cells have known limitations, they are widely used in similar studies and are considered suitable for initial testing.

2 Method

2.1 Chip fabrication

The chip consists of three parts; Figure 4, all cast into a mold. The mold is printed using the Form 3B+ printer (Formlabs, Unites States) with clear V4 resin (Formlabs, United States).

The chip material is a polydimethylsiloxane (PDMS) mixture with a 1:10 ratio curing agent to PDMS, prepared using the Sylgard 184 silicone elastomer kit (Dow, United States). This is poured into the molds and cured overnight in the oven at 60 °C.

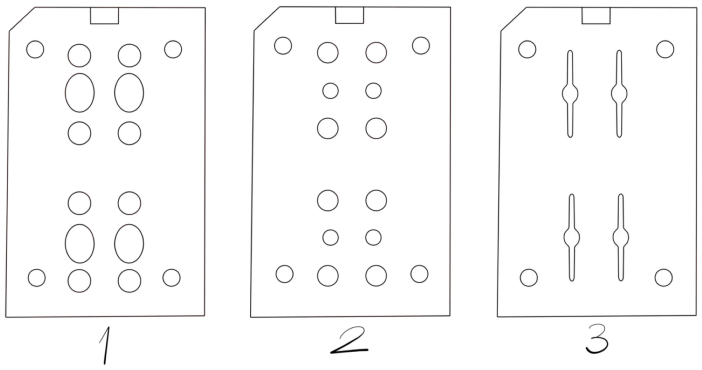

Figure 4: Parts of the chip. 1) show the top layer, 2) middle layer and 3) bottom layer

On the middle part of the chip, a membrane is placed on a silicone waver provided by BIOS and produced as described by M. Zakharova et all [16]. Membrane thickness is 2 μm with a 5 μm pore size, 2% porosity and a seperation of 30 μm between pores.

To apply the membrane, to the middle part, see Figure 4.2, is plasma-treated for 1 minute at 50 Watt in the plasma oven (Henniker plasma, type: HPT-200, United Kingdom) with the membrane. The membrane is then placed onto the middle part and gently pressed down to attach. The part is then placed in the oven for 10 minutes. Next, the middle part is immersed in acetone for 45-60 minutes, covered, to remove the silicone wafer. If the wafer does not detach easily, the soaking time is increased. Afterwards, the middle part is left partially covered overnight to allow evaporation of the absorbed acetone.

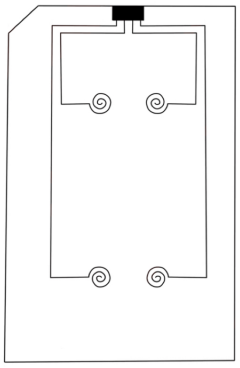

Figure 5: Design of the glass wafer with the electrodes.

The final component of the chip is a glass plate with electrodes obtained from Daniel Wijnperlé (EEMCS-BIOS), see Figure 5. In short, the electrodes are fabricated using Direct Laser Writing (DLW) lithography in a direct laser writing machine (Heidelberg MLA1) on a cleaned 500 μm glass wafer (Mempax, Schott). The wafer is spin-coated with a layer of HMDS followed by a photoresist layer (Olin 1.7 μm). After development using Olin OPD 4262, the wafer is rinsed with DI water and dried. Using a sputtering machine (TCOathy, homemade), a stack of tantalum (4 nm) and platinum (80 nm) is deposited. The tantalum layer acts as an adhesion layer for the platinum. A lift-off process follows where the

sample is soaked in acetone and unwanted metal is lifted away with gentle sonication. The fully detailed protocol can be found in the Appendix ....
To assemble the chip, first the glass plate with the bottom part, see Figure 4.3, is placed in the plasma oven for 1 minute at 50 Watt. The parts are then aligned and rolled down into each other for good attachment. Air bubbles are softly pressed out from under. These steps are repeated for all the parts, placing the middle part on the bottom part and then placing the top part, see Figure 4.1, on the middle part. After the assembly the chip is placed in the oven for 1 hour.

2.2 Cell culture

ARPE-19 cells are cultured in a T75 flask (Sigma-Aldrich, St. Louis, MO, USA) in a medium containing DMEM/F-12 (Gibco, Thermo Fisher Scientific, USA), 10% FBS (Gibco, Thermo Fisher Scientific, USA) and 1% penicillin-streptomycin (pen/strep) (Gibco, Thermo Fisher Scientific, USA).

The chip is placed in the plasma oven for 2 minutes at 50 Watt to sterilize. After sterilization, the chip is immediately coated with sterilized Dopamine-HCl solution (PDA, H8502) with 2 mg/mL dopamine hydrochloride in 10 mM Tris-HCl pH 8.5. This solution is sterilized with a 0.2 μm syringe filter. After coating, the chip is placed in a sterile petri disch wrapped in parafilm and kept at room temperature for 1 hour.

Then the solution is removed and the chip is rinsed 3 times with sterile DPBS (Gibco, Thermo Fisher Scientific, USA), carefully removing all the liquid. The chip is coated with GeltrexTM (A1413201), where the Geltrex is diluted 1:100 in DMEM/F-12. Afterwards, it is placed in the incubator at 37 °C and 5.0% CO_2 for 3 hours.

To detach the ARPE-19, first the medium is removed from the T75 flask and washed once with 5 mL DPBS. After removing the PBS, 1 mL TripLE 1X (ThermoFisher, 12563-011) is added and the flask is placed in the incubator at 37 °C and 5.0 % CO_2 for 5 minutes. To neutralize the TripLE, 5 mL medium is added. The suspension is centrifuged at 300 g for 4 minutes and the supernatant is removed. Then 4 mL medium is added and resuspended where 1 mL of the suspension is used for cell counting. After the 1 mL cell suspension is centrifuged again with the same settings and medium is removed so a cell suspension is made with enough cells to seed 40.000 cells per membrane in 10 μL.

The Geltrex solution is thoroughly removed and without washing 10 μl cell suspension is added to the membrane, while the other channels are filled with medium. The chip is placed in the incubator at 37 °C and 5.0% CO_2 for 30-60 minutes. After incubation, medium is added to fill up the reservoirs.

2.3 Measurements

Since the Locsense Artemis ST system (Locsense, The Netherlands) was redesigned to accommodate the chip, validation tests were performed prior to its use in cell culture experiments. There are four possible positions for placing the chip (A, B, C, and D; see Figure 6b).
In the first test, a chip with a membrane filled with PBS was placed at each of the four positions to assess baseline performance.

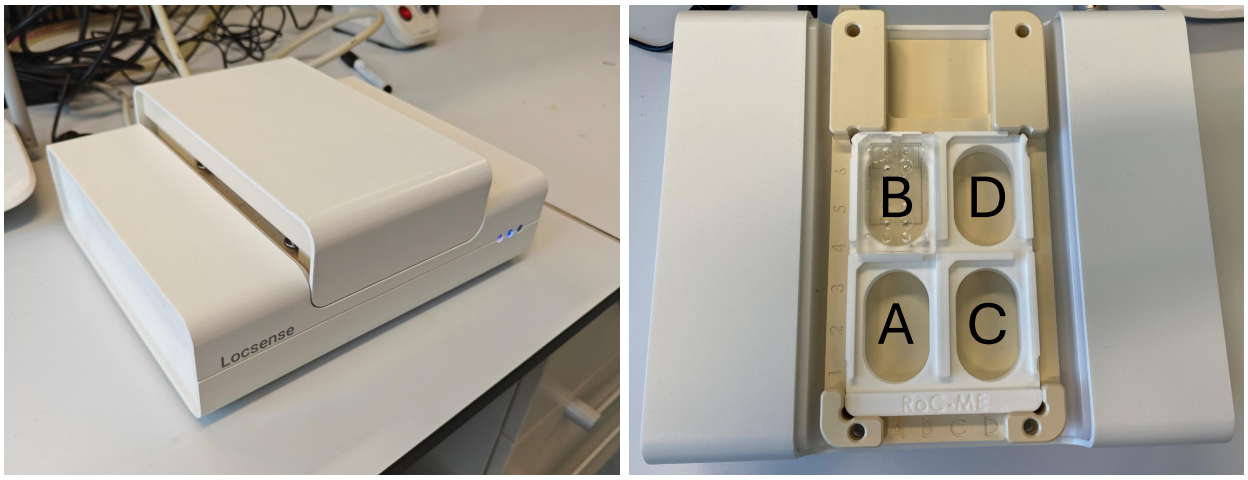

(a) (b)

Figure 6: The Locsense Artemis ST system. (a) The Artemis from the outside with the base and the lid. (b) The holder in the base of the Artemis system for four chips with the possible positions A, B, C and D.

In the second test, both a chip with a membrane and a chip without a membrane were filled with potassium chloride (KCl) solutions prepared by dissolving potassium chloride (P3911-25G, Sigma-Aldrich) in Milli-Q water at concentrations of 10 mM, 100 mM, 500 mM, and 1 M.

Both tests measurements were taken with a frequency sweep form 0 to 100.000 Hz in 20 steps.

After the two test, two experiments with the ARPE-19 were conducted. In the first experiment, a chip with 3 compartments cells cultured on the membrane and one compartment only filled with medium is placed into the Artemis system. Besides this chip two other chips filled with sterile DPBS are also placed into the Artemis to prevent a high evaporation of the medium.

In the second experiment, a second chip (Chip 2) with the same conditions as the first chip is placed, alongside the first chip (Chip 1) and the DPBS filled chips, into the Artemis system. At the end of the two experiments, 14 measurements were conducted for Chip 1 and 7 measurements were conducted for Chip 2.

The lid of the Artemis with the chips is placed into the incubator at 37 °C and 5.0% CO_2. Medium is refreshed three times a week. Measurements are taken before the medium refreshment. Measurements were taken in a 24 hour interval with a frequency sweep from 0 to 10.000 Hz taken in 20 steps.

3 Results

3.1 Tests

Two experimental replicates were conducted for the first test each with 4 measurements (N = 2, n = 4). At a frequency of 100 kHz, where R_{medium} is dominant (Figure 3), the mean impedance magnitude across all compartments and positions in the Artemis was calculated. The results are shown in Figure 7a. Notably, the impedance value differs between positions, with low values observed at positions B and C. The impedance at positions A and D is around 7000 Ohms, while at positions B and C it is approximately 2500 Ohms. The figure also displays individual data points, and at positions B and C, a few high values contribute to large error bars.

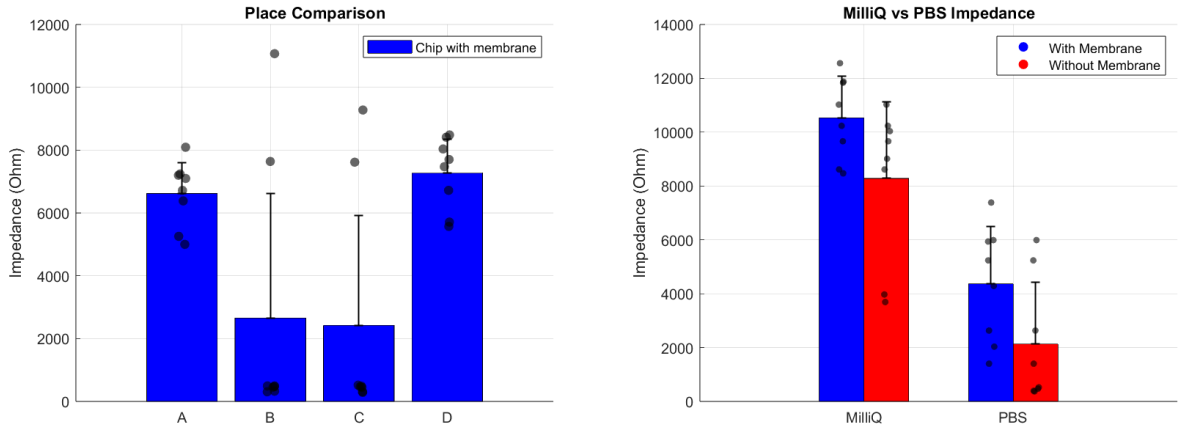

(a) (b)

Figure 7: (a) The impedance magnitude for PBS on the different positions A, B, C and D in the Artemis system, (N = 2, n = 4), (b) The impedance magnitude for MilliQ water and PBS, (N = 2, n = 4).

Two experimental replicates were conducted for the second test each with 4 measurements (N = 2, n = 4). At a frequency of 100 kHz, as selected from the frequency sweep, the mean impedance across the compartments for each KCl concentration was calculated. The results are shown in Figure 8. A chip without a membrane shows a lower impedance value than a chip with a membrane. Furthermore, the impedance value decreases with increasing KCl concentration.

In addition to the second test, a small test was conducted using MilliQ water and PBS. Two experimental replicated were carried out, each with 4 measurements (N = 2, n = 4). The results shown in Figure 7b reflect the impedance values at 100 kHz, as selected from the frequency sweep. It is evident that a chip without a membrane has a lower impedance value. MilliQ has a higher impedance than PBS.

3.2 Cell experiments

For the cell experiments, ARPE-19 cells were seeded onto the membrane in the chip. In Figure 9, panel A shows the membrane without cells, while panel B shows the membrane with ARPE-19 cells on day 12 of the culture. Some linear features are visible, suggesting that cells are present on the membrane; however, proper morphology and confluence are not observed. This includes photos

taken over the cell culture days for both experiments.

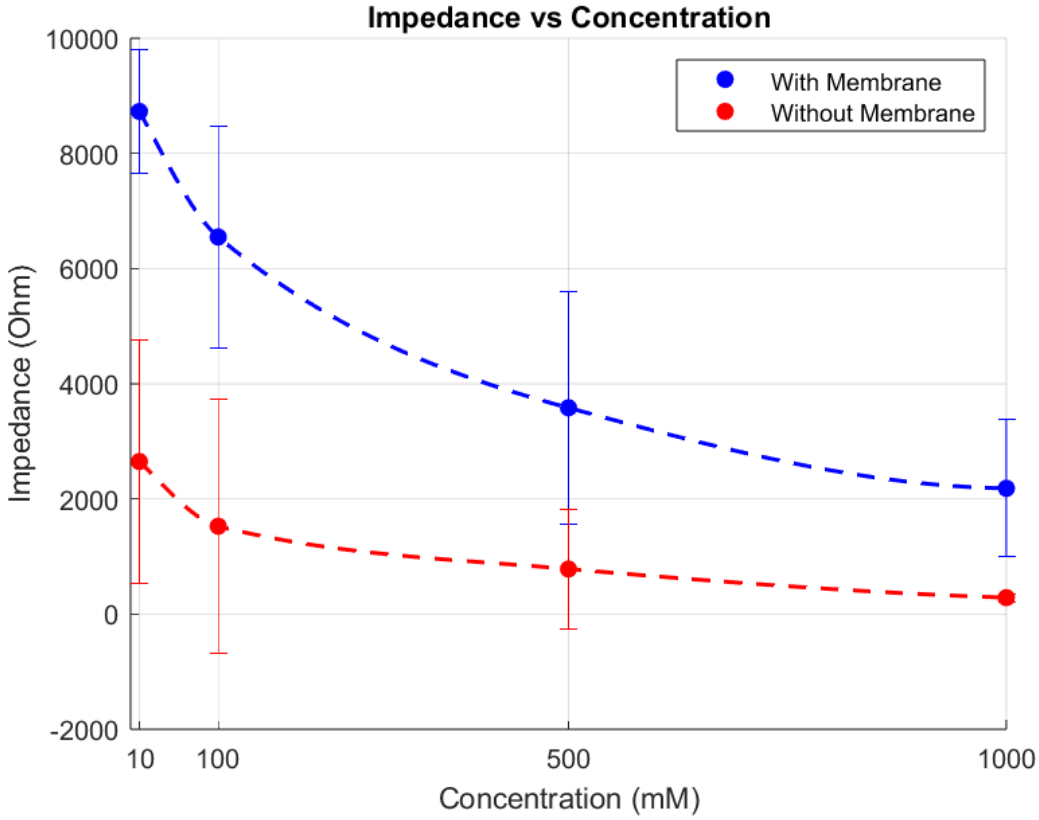

Figure 8: The impedance magnitude at the concentrations 10 mM, 100 mM, 500 mM and 1000 mM KCl for a chip without a membrane (red) and a chip with a membrane (blue), (N = 2, n = 4).

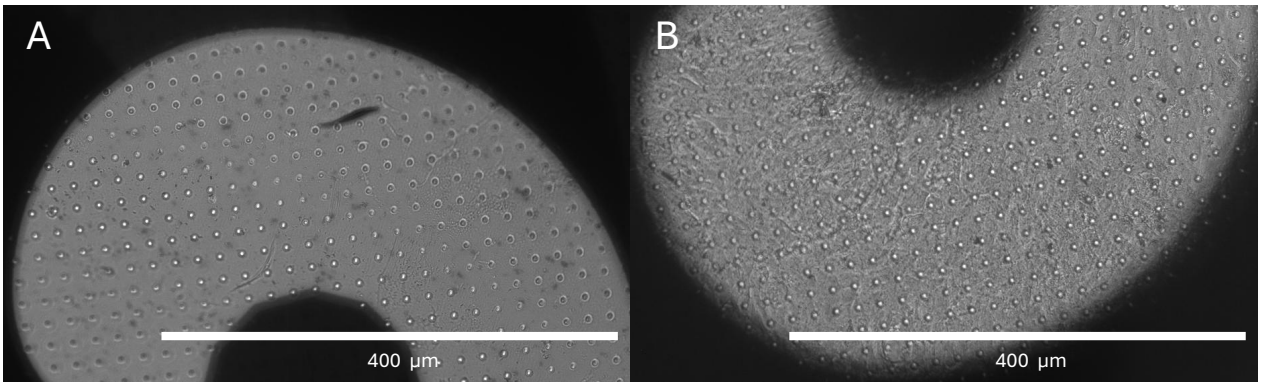

Figure 9: A: The membrane and electrodes of a chip without any cells. B: The membrane with ARPE-19 cells on day 12 of the same chip.

In Figure 10, the results for the second experiment of Chip 2 are shown for different frequencies over 7 days. The frequencies chosen are in the range where R_{TEER} and C_C are dominant (Figure 3). The first noticeable thing is that the impedance value is high, with an order of magnitude of 4 for Figure 10c and 10d and 5 for Figure 10a and 10b. The second thing is that at all the frequencies the impedance value seems to decrease for the first 4 days and an increase again for the last 3 days. For example in Figure 10a there is a high impedance value increase of approximately 40.000 Ohm to day 5 and then a decrease of 20.000 Ohm to day 6 and then an increase of 10.000 Ohm to day 7.

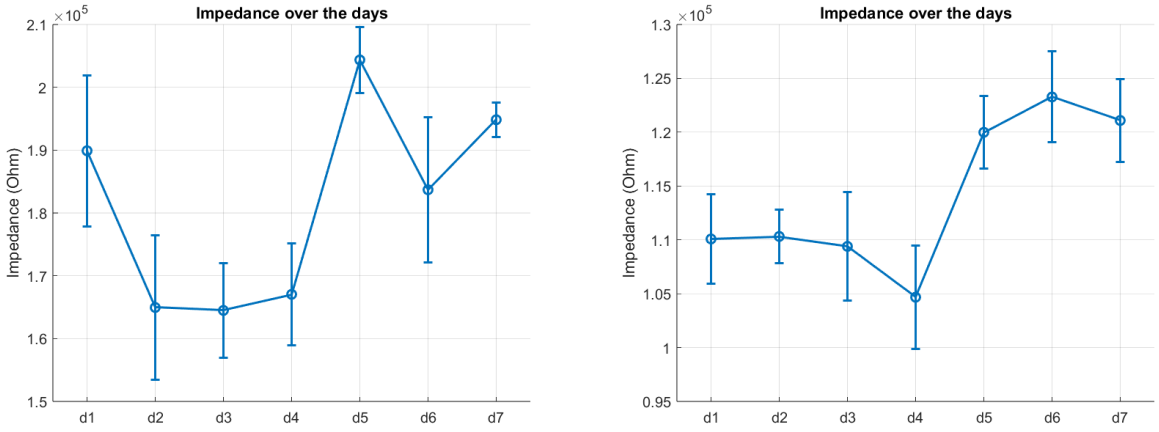

(a) The impedance at the frequency of 5,4 kHz.

(b) The impedance at the frequency of 8,8 kHz.

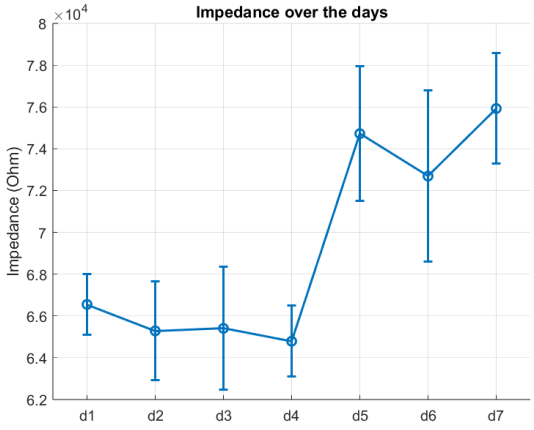

(c) The impedance at the frequency of 14 kHz.

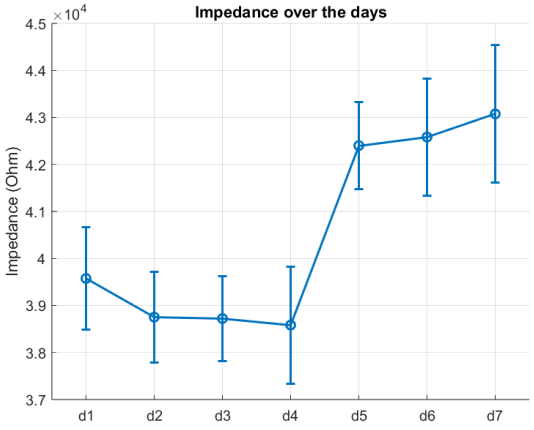

(d) The impedance at the frequency of 23 kHz.

Figure 10: Impedance magnitudes for different frequencies over the days. The x-axis represents days since cell seeding (day 0).

In Figure 11, the results for Chip 1 are shown, combining data from 7 days of the first experiment and 7 days of the second experiment in a single plot across different frequencies. The selected frequencies are within the range where R_{TEER} and C_C are dominant. Similar to the Chip 2, the impedance values mostly decrease during the first 7 days, followed by a sharp increase in the last 3 days. A noticeable increase is also observed from day 5 to day 6. In Appendix A.2 Figure 12 shows the results from the first experiment for a more zoomed in view. The first experiment shows extremely large error bars, whereas the second experiment exhibits much smaller variability.

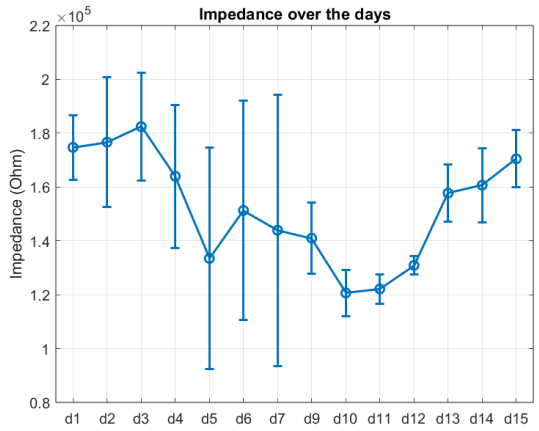

(a) The impedance at the frequency of 5,4 kHz.

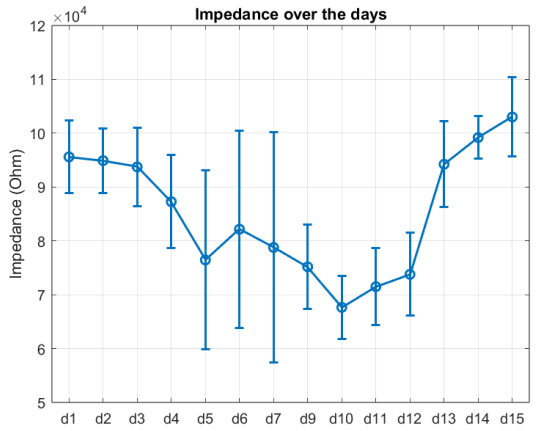

(b) The impedance at the frequency of 8,8 kHz.

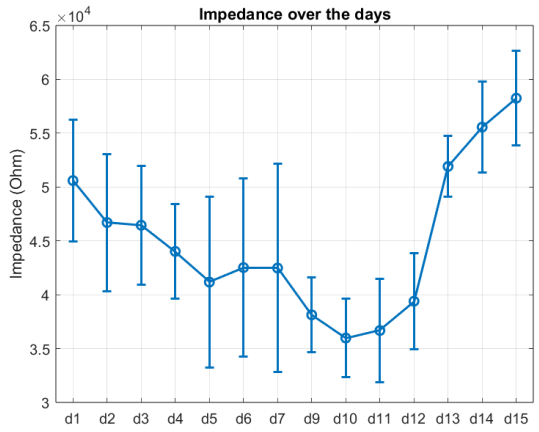

(c) The impedance at the frequency of 14 kHz.

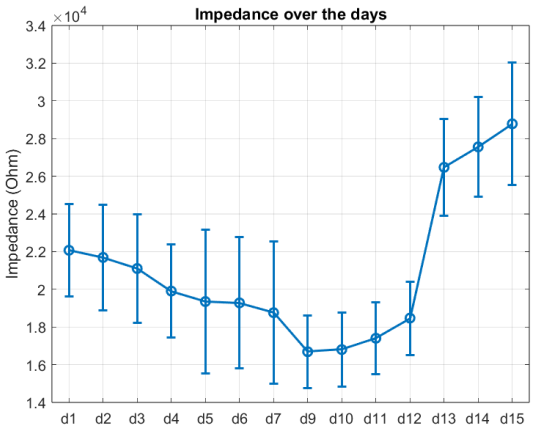

(d) The impedance at the frequency of 23 kHz.

Figure 11: Impedance magnitudes across different frequencies plotted over time. The x-axis represents days since cell seeding (day 0). A total of seven measurements were taken for each experiment, resulting in no measurement on day 8.

4 Discussion

4.1 Impedance differences due to electrode geometry

In all tests and experiments, the results show large error bars. This can be attributed to differences between the compartments. One contributing factor is the variation in the resistance of the ionic solution across compartments. The resistance of the ionic solution depends on the distance between the counter and reference electrodes (l), the cross-sectional area through which current flows (A), and the resistivity of the solution (ρ), as described by Equation 4.1 [17]:

$$R = \rho \frac{l}{A} \tag{4.1}$$

Figure 5 shows that in compartments 2 and 4, the electrode on the glass wafer is longer, resulting in an increased distance l between the counter and reference electrodes. Since ρ and A are assumed to be constant across all compartments, the increased length l leads to a higher resistance, and therefore a higher impedance magnitude [17].

The difference in impedance magnitude is clearly visible in Appendix A.3 Figure 13, specifically in sections a and d, where compartments 2 and 4 exhibit the longer electrode configuration.

However, this is not the only factor contributing to the differences between compartments. For example, the error bars for Chip 1 in the second experiment are reduced compared to those in Experiment 1, indicating that other factors may also be influencing the results. This requires further research.

4.2 Effect of ion concentration and membrane on impedance magnitude

From the results of Test 2, it is clear that a higher ion concentration leads to lower impedance. This is expected, as higher ion concentrations provide more charge carriers, resulting in better conductivity [18]. It also corresponds to lower resistance, and therefore a lower impedance magnitude. The results for MilliQ and PBS further confirm this: MilliQ water contains virtually no ions, resulting in high impedance, while PBS contains dissolved ions and exhibits a lower impedance magnitude.

Test 2 also shows that a chip without a membrane exhibits a lower impedance magnitude. This indicates that the membrane contributes to a higher impedance. This observation aligns with the equivalent electrical circuit shown in Figure 2a, where the membrane introduces an additional resistance term (R_{membrane}).

4.3 High impedance magnitude in ARPE-19 cells

From the results, it is clear that the ARPE-19 cells exhibit a high impedance magnitude. A high impedance magnitude corresponds to a high resistance.

4.3.1 Differentiation and expected impedance magnitude

When ARPE-19 was first reported, they showed many characteristics of well-differentiated primary human RPE's, such as the cobblestone morphology and expression of RPE-specific proteins. How-

ever, after extensive passaging, the well-differentiated culture no longer forms with the commonly-used culture methods. According to R. Hazim et all [19], ARPE-19 cells can be induced to differentiate and express RPE-like characteristics and genes using MEM-Nic medium (MEM alpha with GlutaMAX, 1% FBS, 1% Penicillin/Streptomycin, 1% N1 supplement, taurine (0.25 mg/ml), hydrocortisone (20 ng/ml), triiodo-thyronin (0.013 ng/ml), and 10 mM nicotinamide). However, even with such optimized culture conditions, TEER values remain lower than those observed in native RPE cells [19], indicating a correspondingly lower impedance magnitude.

In this study, standard culture medium was used. The cells did not display the cobblestone morphology, see Appendix A.4 Figure 14, suggesting that the ARPE-19 cells did not resemble primary human RPE. To confirm this, gene analysis is recommended. Based on these observations and prior findings in the literature, a low impedance magnitude would be expected. However, the experiments show high impedance magnitudes, indicating that additional factors may be influencing the results.

4.3.2 Factors related to cell culture

Several factors can affect impedance measurements in cell culture, including temperature, culture duration, and shear stress [7]. The ideal circumstances to determine the TEER value is with a constant temperature of 37 degrees Celsius, so measuring in the incubator. With culture duration it is important to look at the cells forming a monolayer, so cells are not growing on top of each other, and the time it takes to fully form the strong tight junctions. Shear stress on cells can occur when there is flow, changing the impedance magnitude of the cells [7].

In this research, all the measurements were conducted inside the incubator and before medium changes, ruling out the temperature and shear stress as contributing factors. Measurements started directly the day after seeding, so it is possible that the monolayer was not fully formed. A non-confluent monolayer would typically result in a leaky barrier and thus a lower impedance. Multiple studies, all with different medium components, show a fully formed monolayer after 5 to 7 days and a clear increase in the impedance magnitude [20, 21]. This supports the idea that the monolayer was incomplete and prevents ruling out the factor. However, the results show no indications of a leaky barrier and need further research.

4.3.3 Factors related to electrode-electrolyte interface

Other potential explanations for unexpectedly high impedance readings using the Artemis system include dirty electrodes, partially submerged electrodes, or low ion concentrations in the medium [22, 23].

The electrode-containing lid was cleaned with ethanol before initial use, but not in between medium changes. This could mean that the electrodes got dirty [24]. Dirty electrodes reduce the electrode–electrolyte interface, increasing impedance [22, 23, 25]. However, since impedance decreased over time in both experiments (except for the last three days), this seems unlikely to be the primary cause.

The ion concentration in the medium contributes to the conductivity and electrode-electrolyte interface [22, 23, 25]. Over time, ions are taken up by the cells, decreasing their concentration in the

medium. After each medium change, ion levels are replenished, which should temporarily reduce impedance. Therefore, impedance is expected to increase between medium changes and drop after the medium is refreshed. However, the results show a continuous decrease between medium changes and no increase after them. Additionally, the sudden increase in impedance from day 5 to day 6 (see Figure 11) cannot be explained by a medium change, as that occurred only after the day 7 measurement.

The possibility of electrodes not being fully submerged should also be considered. Similar to dirty electrodes, insufficient submersion reduces the effective interface area, increasing impedance [22, 23]. While it cannot be directly observed whether the electrodes were fully submerged, the lid design theoretically ensures this. Furthermore, each compartment was filled completely during every medium change. Although further investigation is necessary to confirm this, precautions were taken to ensure full submersion.

4.3.4 Electrode positioning

One advantage of the Artemis lid is its precise fit, which ensures that the electrodes are reinserted into nearly the same position each time, even after removal. This consistency improves measurement reliability compared to manual electrode repositioning and helps reduce variability between readings.

Finally, in Test 1, all possible electrode placement positions were tested, and it was observed that positions A and D consistently produced higher impedance values. These same positions were used during the cell experiments, which may have contributed to the elevated impedance magnitudes observed.

4.4 Placement in the Artemis system

Since many factors influence impedance, it is difficult to determine the exact cause of the differing values observed for each position in the Artemis system. Most of the factors discussed above could contribute to this variation.

The placement measurements were conducted using a single chip, which was filled at the beginning of the experiment and reused for all four positions. Between each position change, the volume of the chambers was checked and showed no visible signs of drainage. During filling, the chambers were completely, though not excessively, filled, ensuring that the electrodes were fully submerged in PBS. Additionally, the lid of the Artemis was cleaned with ethanol and fully dried before use, ensuring that the pinned electrodes were clean at the start of the measurement.

The measurements were performed at room temperature. While minor variations in temperature may have occurred between tests, these are unlikely to explain the large differences in impedance magnitude observed in a single measurement.

As shown in Appendix A.3 Figure 13 the impedance spectra for positions B and C are clearly different from those of positions A and D.

5 Conclusion

Cell culture factors set the baseline for impedance magnitude, but they do not explain the results observed in this study. ARPE-19 cells, grown in standard medium and lacking cobblestone morphology, are expected to behave as a leaky barrier and produce low impedance values. Additionally, known variables such as temperature, shear stress, or incomplete monolayer formation cannot account for the steady decrease in impedance over time, nor the sudden increase observed in the final three days of the second experiment.

Factors related to the electrode–electrolyte interface, such as dirty electrodes, partial submersion, or low ion concentration, typically lead to an increase in impedance. However, the observed decrease over time suggests these are not the primary causes. In this study, the electrodes were carefully cleaned with ethanol, the chambers were filled completely, and all measurements were conducted inside the incubator under controlled conditions. This makes it unlikely that interface-related issues alone explain the high impedance values seen later in the experiment.

Placement tests revealed that positions A and D consistently produced higher impedance spectra than positions B and C. Since both chips were tested in positions A and D, the variation is likely due to structural or electrical factors related to the Artemis lid. Repeating the placement test with a freshly prepared chip for each position would help isolate positional effects and rule out chip-based variability.

One possible cause of inter-compartment differences is variation in electrode length. To eliminate this variable, an updated glass wafer design with equal-length electrodes has already been implemented (see Appendix A.1). Until the new electrodes are fully validated, a temporary correction factor could be applied during analysis to account for minor differences in electrode geometry.

Future studies should use ARPE-19 cells differentiated with MEM-Nic medium or, preferably, primary or derived RPE lines known to generate higher TEER values. Additional tests should also be conducted to verify consistent electrode submersion and assess the effect of positioning within the Artemis holder. These improvements will help reduce experimental variability and increase confidence in the relationship between impedance magnitude and barrier function.

References

[1] T. Gensheimer, D. Veerman, E. M. van Oosten, L. Segerink, A. Garanto, and A. D. van der Meer. Retina-on-chip: engineering functional in vitro models of the human retina using organ-on-chip technology. *Lab Chip*, 25(5):996–1014, 2025. Gensheimer, Tarek Veerman, Devin van Oosten, Edwin M Segerink, Loes Garanto, Alejandro van der Meer, Andries D eng Review England 2025/01/30 Lab Chip. 2025 Feb 25;25(5):996-1014. doi: 10.1039/d4lc00823e.

[2] R. H. Guymer and T. G. Campbell. Age-related macular degeneration. *Lancet*, 401(10386):1459–1472, 2023. Guymer, Robyn H Campbell, Thomas G eng Research Support, Non-U.S. Gov't Review England 2023/03/31 Lancet. 2023 Apr 29;401(10386):1459-1472. doi: 10.1016/S0140-6736(22)02609-5. Epub 2023 Mar 27.

[3] E. K. Markert, H. Klein, C. Viollet, W. Rust, B. Strobel, S. G. Kauschke, B. Makovoz, H. Neubauer, R. A. Bakker, and T. A. Blenkinsop. Transcriptional comparison of adult human primary retinal pigment epithelium, human pluripotent stem cell-derived retinal pigment epithelium, and arpe19 cells. *Front Cell Dev Biol*, 10:910040, 2022. Markert, Elke K Klein, Holger Viollet, Coralie Rust, Werner Strobel, Benjamin Kauschke, Stefan G Makovoz, Bar Neubauer, Heike Bakker, Remko A Blenkinsop, Timothy A eng Switzerland 2022/09/13 Front Cell Dev Biol. 2022 Aug 26;10:910040. doi: 10.3389/fcell.2022.910040. eCollection 2022.

[4] L. Liu and X. Liu. Roles of drug transporters in blood-retinal barrier. *Adv Exp Med Biol*, 1141:467–504, 2019. Liu, Li Liu, Xiaodong eng Review 2019/10/02 Adv Exp Med Biol. 2019;1141:467-504. doi: 10.1007/978-981-13-7647-$4_1$0.

[5] C. Ma, Y. Peng, H. Li, and W. Chen. Organ-on-a-chip: A new paradigm for drug development. *Trends Pharmacol Sci*, 42(2):119–133, 2021. Ma, Chao Peng, Yansong Li, Hongtong Chen, Weiqiang eng Research Support, N.I.H., Extramural Review England 2020/12/21 Trends Pharmacol Sci. 2021 Feb;42(2):119-133. doi: 10.1016/j.tips.2020.11.009. Epub 2020 Dec 16.

[6] U. M. N. Cao, Y. Zhang, J. Chen, D. Sayson, S. Pillai, and S. D. Tran. Microfluidic organ-on-a-chip: A guide to biomaterial choice and fabrication. *Int J Mol Sci*, 24(4), 2023. Cao, Uyen M N Zhang, Yuli Chen, Julie Sayson, Darren Pillai, Sangeeth Tran, Simon D eng Review Switzerland 2023/02/26 Int J Mol Sci. 2023 Feb 6;24(4):3232. doi: 10.3390/ijms24043232.

[7] B. Srinivasan, A. R. Kolli, M. B. Esch, H. E. Abaci, M. L. Shuler, and J. J. Hickman. Teer measurement techniques for in vitro barrier model systems. *J Lab Autom*, 20(2):107–26, 2015. Srinivasan, Balaji Kolli, Aditya Reddy Esch, Mandy Brigitte Abaci, Hasan Erbil Shuler, Michael L Hickman, James J eng UH2 TR000516/TR/NCATS NIH HHS/ UH2TR000516/TR/NCATS NIH HHS/ Research Support, N.I.H., Extramural Review 2015/01/15 J Lab Autom. 2015 Apr;20(2):107-26. doi: 10.1177/2211068214561025. Epub 2015 Jan 13.

[8] J. Liu, W. Zhao, M. Qin, X. Luan, Y. Li, Y. Zhao, C. Huang, L. Zhang, and M. Li. Real-time measurement of the trans-epithelial electrical resistance in an organ-on-a-chip during cell proliferation. *Analyst*, 148(3):516–524, 2023. Liu, Jinlong Zhao, Wenjie Qin, Meiyan Luan, Xiaofeng Li, Yuang Zhao, Yang Huang, Chengjun Zhang, Lingqian Li, Mingxiao eng England 2023/01/11 Analyst. 2023 Jan 31;148(3):516-524. doi: 10.1039/d2an01931k.

[9] M. Malik, S. A. Steele, D. Mitra, C. J. Long, and J. J. Hickman. Trans-epithelial/endothelial electrical resistance (teer): Current state of integrated teer measurements in organ-on-a-chip devices.

Curr Opin Biomed Eng, 34, 2025. Malik, Mridu Steele, Stecia A Mitra, Deepshikha Long, Christopher J Hickman, James J eng England 2025/04/25 Curr Opin Biomed Eng. 2025 Jun;34:100588. doi: 10.1016/j.cobme.2025.100588. Epub 2025 Mar 19.

[10] K. Benson, S. Cramer, and H. J. Galla. Impedance-based cell monitoring: barrier properties and beyond. *Fluids Barriers CNS*, 10(1):5, 2013. Benson, Kathrin Cramer, Sandra Galla, Hans-Joachim eng England 2013/01/12 Fluids Barriers CNS. 2013 Jan 10;10(1):5. doi: 10.1186/2045-8118-10-5.

[11] Y. Shi, S. Sun, H. Liu, M. Zhao, M. Qin, J. Liu, J. Hu, Y. Zhao, M. Li, L. Zhang, and C. Huang. Real-time cell barrier monitoring by spatial transepithelial electrical resistance measurement on a microelectrode array integrated transwell. *Lab Chip*, 25(2):253–262, 2025. Shi, Yimin Sun, Sheng Liu, Hui Zhao, Mingda Qin, Meiyan Liu, Jinlong Hu, Jingfang Zhao, Yang Li, Mingxiao Zhang, Lingqian Huang, Chengjun eng England 2024/12/17 Lab Chip. 2025 Jan 14;25(2):253-262. doi: 10.1039/d4lc00817k.

[12] P. Zoio and A. Oliva. Skin-on-a-chip technology: Microengineering physiologically relevant in vitro skin models. *Pharmaceutics*, 14(3), 2022. Zoio, Patricia Oliva, Abel eng Review Switzerland 2022/03/27 Pharmaceutics. 2022 Mar 21;14(3):682. doi: 10.3390/pharmaceutics14030682.

[13] J. Yeste, X. Illa, M. Alvarez, and R. Villa. Engineering and monitoring cellular barrier models. *J Biol Eng*, 12:18, 2018. Yeste, Jose Illa, Xavi Alvarez, Mar Villa, Rosa eng Review England 2018/09/15 J Biol Eng. 2018 Sep 12;12:18. doi: 10.1186/s13036-018-0108-5. eCollection 2018.

[14] O. Y. F. Henry, R. Villenave, M. J. Cronce, W. D. Leineweber, M. A. Benz, and D. E. Ingber. Organs-on-chips with integrated electrodes for trans-epithelial electrical resistance (teer) measurements of human epithelial barrier function. *Lab Chip*, 17(13):2264–2271, 2017. Henry, Olivier Y F Villenave, Remi Cronce, Michael J Leineweber, William D Benz, Maximilian A Ingber, Donald E eng Research Support, N.I.H., Extramural Research Support, U.S. Gov't, Non-P.H.S. England 2017/06/10 Lab Chip. 2017 Jun 27;17(13):2264-2271. doi: 10.1039/c7lc00155j.

[15] D. Marrero, A. Guimera, L. Maes, R. Villa, M. Alvarez, and X. Illa. Organ-on-a-chip with integrated semitransparent organic electrodes for barrier function monitoring. *Lab Chip*, 23(7):1825–1834, 2023. Marrero, Denise Guimera, Anton Maes, Laure Villa, Rosa Alvarez, Mar Illa, Xavi eng Research Support, Non-U.S. Gov't England 2023/02/23 Lab Chip. 2023 Mar 28;23(7):1825-1834. doi: 10.1039/d2lc01097f.

[16] Mariia Zakharova, Martijn P. Tibbe, Lena S. Koch, Hai Le-The, Anne M. Leferink, Albert van den Berg, Andries D. van der Meer, Kerensa Broersen, and Loes I. Segerink. Transwell-integrated 2 µm thick transparent polydimethylsiloxane membranes with controlled pore sizes and distribution to model the blood-brain barrier. *Advanced Materials Technologies*, 6(12), 2021.

[17] n.k. Basics of electrochemical impedance spectroscopy, n.k.

[18] Qing Huang, Qizhao Luo, Zhe Chen, Lei Yao, Ping Fu, and Zhidong Lin. The effect of electrolyte concentration on electrochemical impedance for evaluating polysulfone membranes. *Environmental Science: Water Research Technology*, 4(8):1145–1151, 2018.

[19] R. A. Hazim, S. Volland, A. Yen, B. L. Burgess, and D. S. Williams. Rapid differentiation of the human rpe cell line, arpe-19, induced by nicotinamide. *Exp Eye Res*, 179:18–24, 2019. Hazim, Roni A Volland, Stefanie Yen, Alice Burgess, Barry L Williams, David S eng Research Support, N.I.H., Extramural England 2018/10/20 Exp Eye Res. 2019 Feb;179:18-24. doi: 10.1016/j.exer.2018.10.009. Epub 2018 Oct 15.

[20] Z. Ablonczy, M. Dahrouj, P. H. Tang, Y. Liu, K. Sambamurti, A. D. Marmorstein, and C. E. Crosson. Human retinal pigment epithelium cells as functional models for the rpe in vivo. *Invest Ophthalmol Vis Sci*, 52(12):8614–20, 2011. Ablonczy, Zsolt Dahrouj, Mohammad Tang, Peter H Liu, Yueying Sambamurti, Kumar Marmorstein, Alan D Crosson, Craig E Research Support, N.I.H., Extramural Research Support, Non-U.S. Gov't 2011/10/01 Invest Ophthalmol Vis Sci. 2011 Nov 4;52(12):8614-20. doi: 10.1167/iovs.11-8021.

[21] S. A. Lynn, E. Keeling, J. M. Dewing, D. A. Johnston, A. Page, A. J. Cree, D. A. Tumbarello, T. A. Newman, A. J. Lotery, and J. A. Ratnayaka. A convenient protocol for establishing a human cell culture model of the outer retina. *F1000Res*, 7:1107, 2018. Lynn, Savannah A Keeling, Eloise Dewing, Jennifer M Johnston, David A Page, Anton Cree, Angela J Tumbarello, David A Newman, Tracey A Lotery, Andrew J Ratnayaka, J Arjuna 2018 Jul 18;7:1107. doi: 10.12688/f1000research.15409.1. eCollection 2018.

[22] W. Franks, I. Schenker, P. Schmutz, and A. Hierlemann. Impedance characterization and modeling of electrodes for biomedical applications. *IEEE Trans Biomed Eng*, 52(7):1295–302, 2005. Franks, Wendy Schenker, Iwan Schmutz, Patrik Hierlemann, Andreas eng Evaluation Study Research Support, Non-U.S. Gov't Validation Study 2005/07/27 IEEE Trans Biomed Eng. 2005 Jul;52(7):1295-302. doi: 10.1109/TBME.2005.847523.

[23] Henry S. White. Allen J. Bard, Larry R. Faulkner. *Electrochemical methods : fundamentals and applications*. Hoboken, NJ : John Wiley Sons, Ltd., third edition, 2022.

[24] PhD Subhra Nag. How to troubleshoot teer measurement problems, n.k.

[25] Andrea Mulligan. Why electrodes matter: Electrode-electrolyte interface, n.k.

A Appendix

A.1 Full protocol for glass wafer

Below is the full protocol for the glass wafer. On the first page is a schematics with equal electrode lengths for each compartment. This is an updated version of the glass wafer which was not available at the time of this research. For the glass wafer of this research see Figure 5.

Layout

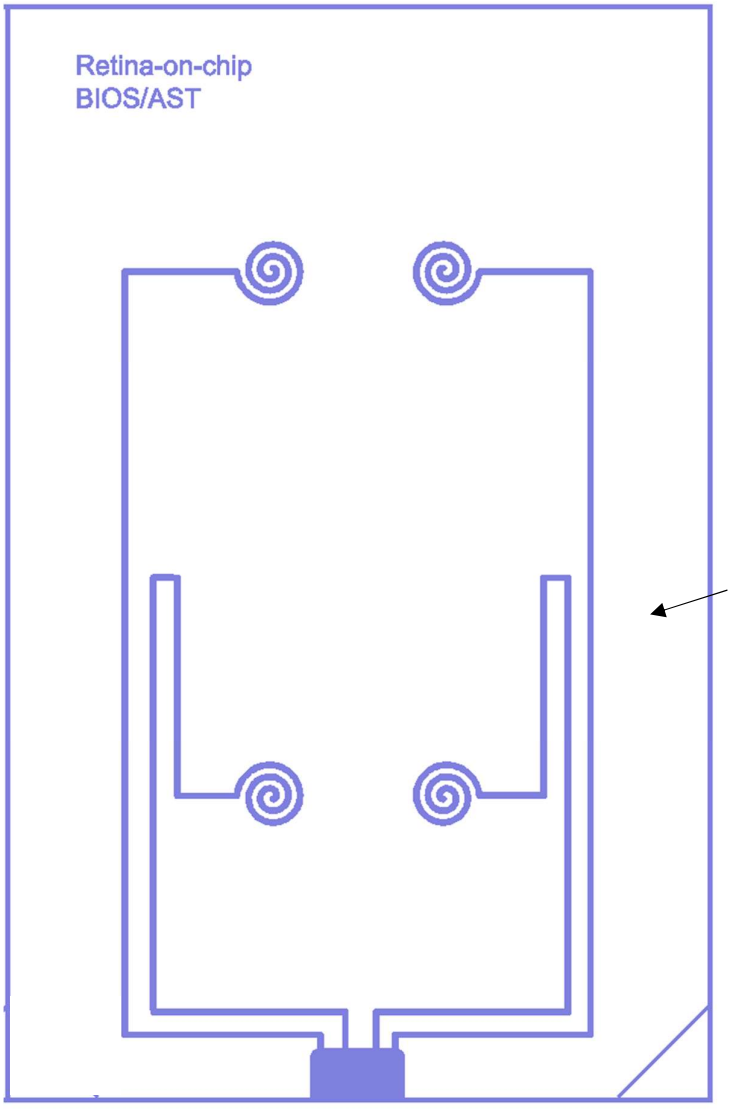

Fig 1. Chipdesign

Process description

The electrodes are made by Direct Laser Writing (DLW) lithography**.** First, the substrate (*2a*) which is 500 um glasswafer (Mempax, Schott) is thoroughly cleaned by soaking it in nitric acid (99%) for 5 minutes, followed by rinsing in deionized water and spindrying. Once clean, a 10 minute dehydration bake is performed at a temperature of 120°C on a hotplate. Prior to spincoating the photoresist layer (Olin 1.7um), a layer of HMDS is spincoated, ensuring a good adhesion of the photoresist (*2b*). After a softbake at 95°C for 1 minute on a hotplate, the wafer is ready for exposure in a direct laser writing machine (Heidelberg MLA1).

Once the design of the electrode pattern is loaded to the machine, the laser writes the pattern directly onto the resist with high precision. After exposure, the sample is developed (Olin OPD 4262) rinsed in DI water and dried (*2c*).

Following pattern development, a stack of Tantalum (4 nm) and Platinum (80 nm) is deposited using a sputtering machine (TCOathy, homemade). The Tantalum layer acts as an adhesion layer for the Platinum layer (*2d*). Finally, lift-off is performed by soaking the sample in acetone. With gentle sonication, the unwanted metal lifts away along with the resist, leaving behind clean, well-defined electrodes (*2e*). After a final rinse and inspection under a microscope, the glasswafer is diced (Disco DAD3220) in individual chips.

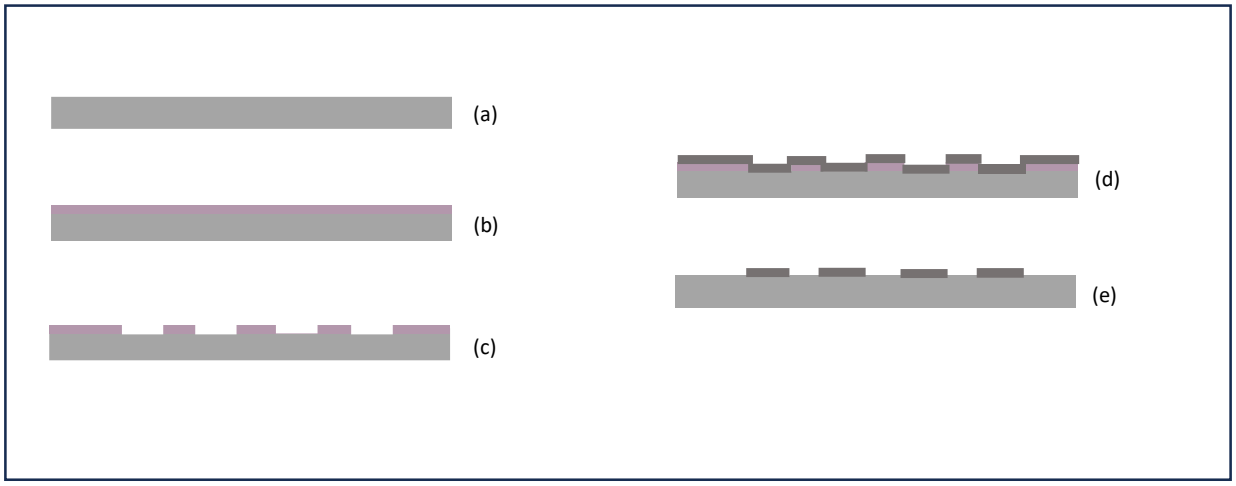

Fig 2. Schematic of the process

Process Flow

ILP: In-line Processing	MFP: Metal-free Processing	UCP: Ultra Clean Processing	Removal of Residues

Step	Level	Process/Basic flow		User comments
1		**Substrate MEMpax** (#subs117)	NL-CLR-Cupboard Diameter: 100mm Thickness: 500µm	
		clean1002: In-line cleaning (WB16-ILP)		
2	ILP	**Cleaning in 99% HNO3** (#clean005)	**NL-CLR-WB16 BEAKER 1** Purpose: removal of organic traces. Chemical: 99% HNO3 • Time: 5min NOTE: only dry wafers are allowed to enter this beaker in order to prevent dilution of the 99% HNO3!	be careful, wafers are fragile!
3	ILP	**Cleaning in 99% HNO3** (#clean006)	**NL-CLR-WB16 BEAKER 2** Purpose: removal of organic traces. Chemical: 99% HNO3 • Time: 5min	
4	ILP	**Rinsing** (#rinse001)	**NL-CLR-WBs QDR** Purpose: removal of traces of chemical agents. Choose one of the two rinsing modes: **QDR** = Quick dump rinsing mode **Cascade** = Overflow rinsing mode for fragile substrates Rinse until message ´End of rinsing process´ is shown on the touchscreen of the QDR, else repeat the rinsing process.	
5	ILP	**Substrate drying** (#dry001)	**NL-CLR-WBs (ILP)** Single substrate drying: 1. Use the single-wafer spinner Settings: 2500 rpm, 60 sec (including 45 sec nitrogen purge) 2. Use the nitrogen gun (fragile wafers or small samples)	

litho1801: Lithography of Olin Oir 907-17 (positive resist - ILP)

6	ILP	**HMDS priming** (#litho600)	**OPTION 1 Liquid HMDS priming** **NL-CLR-WB21/22 HOTPLATE** Purpose: dehydration bake Settings: • Temperature: 120°C • Time: 5min After the dehydration bake, perform the liquid priming with minimum delay! **NL-CLR-WB21 Primus SB15 Spinner** Primer: HexaMethylDiSilazane (HMDS) Settings: • Spin mode: static • Spin speed: 4000rmp • Spin time: 30s **OPTION 2 Vapor HMDS priming** **NL-CLR-WB28 Lab-line Duo-Vac Oven** Primer: HexaMethylDiSilazane (HMDS) Settings: • Temperature: 150°C • Pressure: 25inHg • Dehydratation bake: 2min • HMDS priming: 5min CAUTION: let the substrates cool down before handling with your tweezer!
7	ILP	**Coating of Olin OiR 907-17** (#litho101)	**NL-CLR-WB21 PRIMUS SB15 SPINNER** Resist: Olin OiR 907-17 Spin program: 4000 Settings: • Spin mode: static • Spin speed: 4000rpm • Spin time: 30s
8	ILP	**Prebake of Olin OiR 907-17** (#litho003)	**NL-CLR-WB21 PREBAKE HOTPLATE** Purpose: removal of residual solvent from the resist film after spin coating. Settings: • Temperature: 95°C • Time: 90s
9	ILP	**Direct Laser Writing (MLA)** (#litho301)	**NL-CLR-Heidelberg MLA** Settings:(MLA1) • Exposure dose: 150 mJ/cm^2 • Laser: 375 nm

10	ILP	**Development of Olin OiR resists** (#litho200)	**NL-CLR-WB21 DEVELOPMENT BEAKERS** Developer: OPD4262 • Beaker 1: 30sec • Beaker 2: 15-30sec
11	ILP	**Rinsing** (#rinse001)	**NL-CLR-WBs QDR** Purpose: removal of traces of chemical agents. Choose one of the two rinsing modes: **QDR** = Quick dump rinsing mode **Cascade** = Overflow rinsing mode for fragile substrates Rinse until message ´End of rinsing process´ is shown on the touchscreen of the QDR, else repeat the rinsing process.
12	ILP	**Substrate drying** (#dry001)	**NL-CLR-WBs (ILP)** Single substrate drying: 1. Use the single-wafer spinner Settings: 2500 rpm, 60 sec (including 45 sec nitrogen purge) 2. Use the nitrogen gun (fragile wafers or small samples)
13	ILP	**Postbake of Olin OiR resists** (#litho008)	**NL-CLR-WB21 POSTBAKE HOTPLATE** Purpose: Settings: • Temperature: 120°C • Time: 10min
14	ILP	**Inspection by Optical Microscopy** (#metro101)	**NL-CLR-Nikon Microscope** Use the Nikon microscope for inspection.

film1631: Sputtering of Tantalum (TCOathy)

15	ILP	**Sample preparation** (#film631)	**NL-CLR-T´COathy** Purpose: reduce outgassing and pump time. - Use a dehydration bake (120°C, 5 mins) in WB22 after wet processing. - Use only Kapton tape for fixing samples on a carrier wafer or a shadow mask* on a process wafer. *TCO is the preferred supplier of shadow masks.

16 ILP **Sputtering of Ta** (#film633)

NL-CLR-T´COathy
Application: deposition of Tantalum

thickness ~ 5 nm --> time 30 sec

• Base pressure: <1.0E-6 mbar

Layer	Target	Power (W)	Pre-time	Proc-time	P (x10-3) mbar
	Ta	200	1:00	0:30	6.6

• Deposition rate ~ 10 nm/min

film1604: Sputtering of Platinum (Sputterke)

17 ILP **Sample preparation** (#film600)

NL-CLR-SPUTTERKE
Purpose: reduce outgassing and pump time.

- Only use Kapton tape for fixing small samples on the carrier or for fixing a shadow mask*
- Advise: use a dehydration bake (120°C, 5 mins) in WB22 after wet processing

*TCO is the preferred supplier of shadow masks.

18 ILP **Presputtering** (#film601)

NL-CLR-SPUTTERKE
Purpose: process stabilization and removal of surface contamination from 2 inch sputter targets without deposition on the substrate.

Target (gun #: see MIS logbook)
Note: point the shutter away from the selected gun!

Settings:
• Ar flow: same as process
• Base pressure: <2.0e-6mbar
• Process pressure: same as process
• Power: same as process
• Process step time: 60s

19	ILP	**Sputtering of Pt** (#film605)	**NL-CLR-SPUTTERKE** Application: deposition of Platinum. **RESTRICTION**: Au and Pt depositions are assigned to T'COathy. Exceptions can be made for specific material combinations and/or incompatible samples sizes. Discuss with the system administrator! Settings: • Target: Pt (gun #: see MIS logbook) • Ar flow: adjust the argon flow to set the process pressure • Base pressure: < 2.0 e-6mbar • Process pressure: 6.6 e-3mbar • Power: 200W • Estimated deposition rate: 45-50nm/min. Check the current deposition rate in the digital logbook or perform a rate calibration first. **Please note:** this sputter recipe suffices to deposit a film of Gold. To obtain specific film properties contact the system administrator to discuss the process parameter settings.	thickness ~80 nm --> time 3:30 min

litho1500: Lift-Off with postive resists (WB11)

20	ILP	**Lift-Off** **(**#litho500)	**NL-CLR-WB11 ULTRASONIC BATH** Purpose: removal of resist and excess metal from the surface of the substrate by ultrasonication in Acetone. • Beaker 1: Acetone • Time = 10 min **Single wafer processing:** Spray the wafer with Acetone for 30 sec and immediately spray with isopropanol (IPA) for 30 sec. **Batch wafer processing:** • Beaker 2: Acetone • Time = 10 min • Beaker 3: Isopropanol • Time = 10 min	utrasonic for 2 min then leave overnight
21	ILP	**Substrate drying** (#dry001)	**NL-CLR-WBs (ILP)** Single substrate drying: 1. Use the single-wafer spinner Settings: 2500 rpm, 60 sec (including 45 sec nitrogen purge) 2. Use the nitrogen gun (fragile wafers or small samples)	
22	ILP	**Inspection by Optical Microscopy** (#metro102)	**NL-CLR-Optical Microscopes** Use one of the Olympus microscopes for inspection.	

metro1101: Inspection by Optical Microscopy (Olympus)

23	ILP	**Inspection by Optical Microscopy** (#metro102)	**NL-CLR-Optical Microscopes** Use one of the Olympus microscopes for inspection.

back1101: Dicing of glass wafer

24	ILP	**UV dicing foil (Adwill D-210)** (#back104)	Nl-CLR- Dicing foil Information: Thickness: 125um Material: 100um PET + 25um Acrylic (adhesive) Adhesion before UV: 2000 mN/25mm Adhesion after UV : 15 mN/25mm UV irradiation : Luminance > 120mW/cm^2 and Quality > 70mJ/cm^2 (wave length: 365nm)
25	ILP	**Dicing foil Nitto SWT 10** (#back103)	NL-CLR dicingroom Nitto SWT 10 dicing foil
26	ILP	**Dicing of a glass wafer** (#back102)	**NL-CLR-Dicing room** Use Disco DAD dicing saw or Load point Micro Ace 3 Applications: Borofloat, Fused silica or Pyrex wafers and Silicon wafers bonded on Borofloat, Fused silica or Pyrex See #back103 for laminate of Nitto STW T10 dicing foil See #back104 for laminate of UV dicing foil **Parameters dicing:** Wafer work size: 110 mm for a standard 100 mm silicon wafer Shape: square for square wafers Feed speed: 6 mm/sec (for 500um cut depth) Feed speed: 4 mm/sec (for 1000um cut depth) Max cut depth: 1000um per cycle X, Y values: correspond respectively to Ch1 and Ch2 and those values are determined by mask layout Saw type TC300 Select in blade menu: **2.187-12A** **Blade info:** Exposure: 3 mm (maximum dicing depth for a new blade) Width: 300 um Spindle revolutions: ; 25. 000 rpm **Depth settings:** Maximum cut depth: 1.0 mm at a time (per cycle/run) Foil thickness: See foil info Min. blade heigth: 50 µm

A.2 Results first experiment

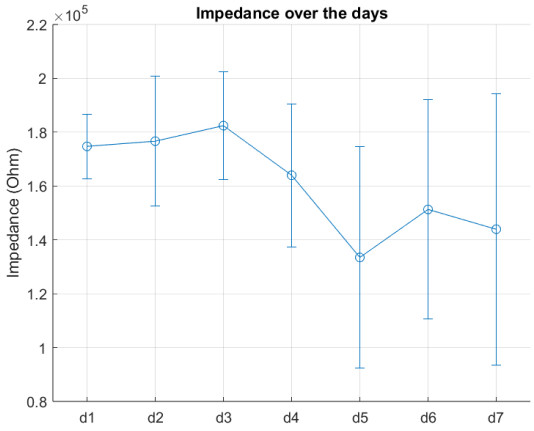

(a) The impedance at the frequency of 5,4 kHz.

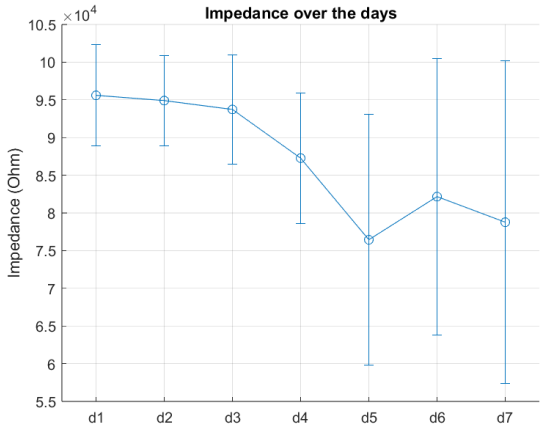

(b) The impedance at the frequency of 8,8 kHz.

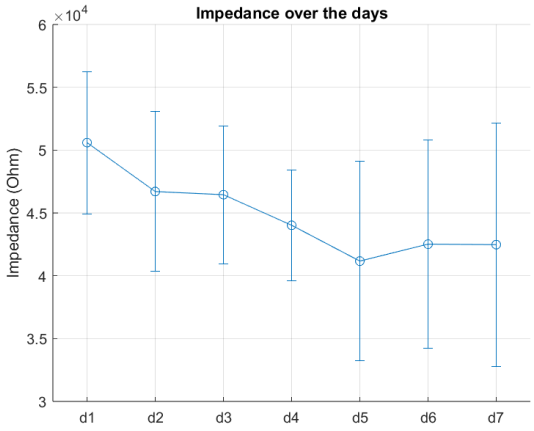

(c) The impedance at the frequency of 14 kHz.

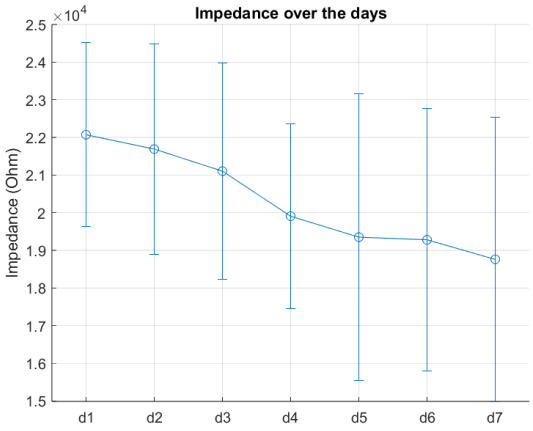

(d) The impedance at the frequency of 23 kHz.

Figure 12: Impedance magnitudes for different frequencies over the days. The x-axis represents days since cell seeding (day 0).

A.3 Impedance spectrum placement test

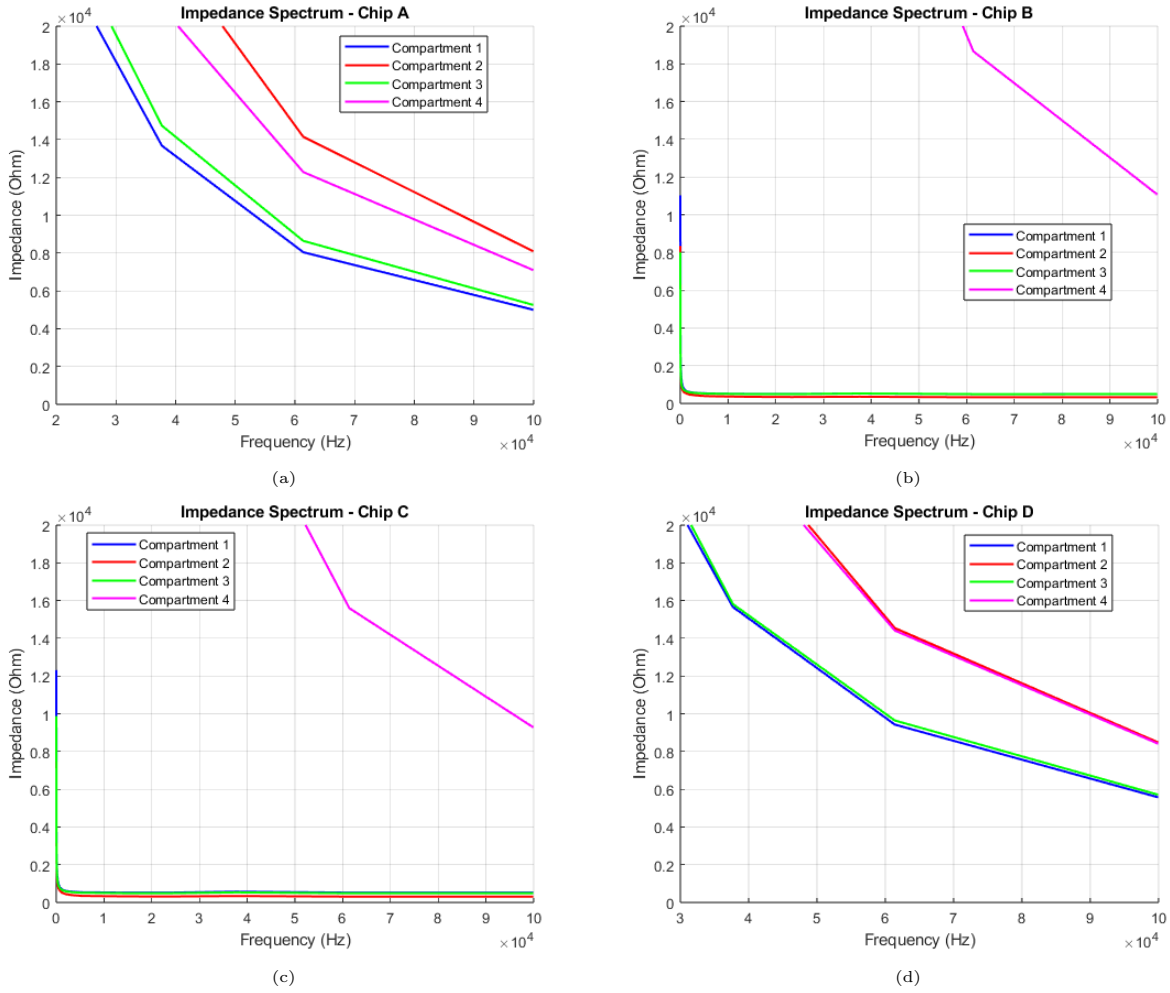

(a) (b) (c) (d)

Figure 13: Impedance spectrum for each position in the Artemis system, with a to d representing position A to D.

A.4 ARPE-19 cells

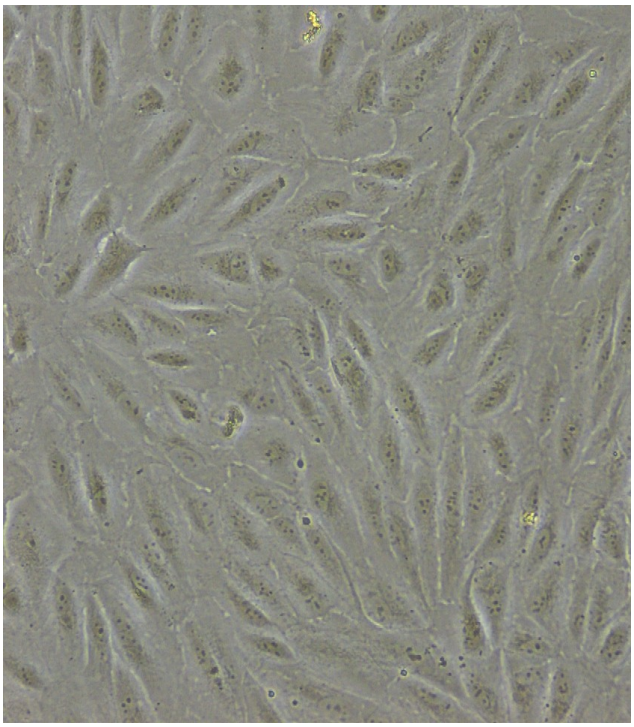

Figure 14: The ARPE-19 cells in the T75 flask, showing no cobblestone morphology.